metals

MDPI

Article

Microwave Treatment of Copper–Nickel Sulfide Ore for Promotion of Grinding and Flotation

Xiaolei Fang, Zhiwei Peng *, Tianle Yin, Mingjun Rao and Guanghui Li

School of Minerals Processing and Bioengineering, Central South University, Changsha 410083, China
* Correspondence: zwpeng@csu.edu.cn; Tel.: +86-731-88877656

Abstract: The effect of microwave treatment on the grinding and flotation performance of a typical copper–nickel sulfide ore was evaluated, based on the determination of its microwave absorption capability, grinding and flotation indexes such as crack percentage, mineral liberation degree, particle size distribution, relative work index (RWI), metal enrichment ratio and recovery. There were obvious differences between the microwave absorption capabilities of the main minerals in the ore, as demonstrated by their different microwave penetration depths. They also induced temperature differences between sulfide minerals and gangue minerals which could reach 418 °C after microwave treatment for 20 s. It was shown that microwave treatment could effectively improve the grindability of the ore, as proven by the increase in fine particles smaller than 0.074 mm and the decrease in RWI after grinding due to the higher crack percentage and mineral liberation degree. Moreover, microwave treatment affected the ore floatability because of the generation of cuprite, retgersite, and rozenite with poor floatability when the treatment time was extended. By microwave treatment for a proper time, 20 s, an optimal balance between the grindability and flotation performance could be achieved. Compared with the untreated ore, the RWI of the ore decreased by 11.5%. After flotation, the Cu and Ni enrichment ratios of the flotation concentrate increased by 0.3 and 0.2, respectively. Meanwhile, their corresponding recoveries increased by 4.2% and 3.1%. This study provides new insights for the treatment of copper–nickel sulfide ore to enhance the grinding and flotation process.

Keywords: microwave treatment; copper–nickel sulfide ore; thermodynamics; grinding indexes; flotation

Citation: Fang, X.; Peng, Z.; Yin, T.; Rao, M.; Li, G. Microwave Treatment of Copper–Nickel Sulfide Ore for Promotion of Grinding and Flotation. *Metals* **2024**, *14*, 565. https://doi.org/10.3390/met14050565

Academic Editors: Ilhwan Park and Sanghee Jeon

Received: 19 March 2024
Revised: 2 May 2024
Accepted: 7 May 2024
Published: 11 May 2024

1. Introduction

Nickel is an important strategic metal with high temperature and corrosion resistances, high ferromagnetism, and good plasticity [1]. It has important applications in stainless steel, batteries, high temperature alloys, catalysts, etc. [2,3]. The current sources of nickel ore for industrial applications in the world are nickel sulfide ore and nickel laterite ore [4]. The Jinchuan deposit is the third largest magmatic copper–nickel sulfide deposit in the world and the largest one in China [5]. In general, increasing the grade of nickel sulfide ore for smelting is important for the full utilization of the resource [6]. With the continuous mining of nickel sulfide ore, the proportion of low-grade ore keeps increasing [7]. To meet the smelting requirements of nickel sulfide ore, a preliminary mineral concentration by flotation is often required [8]. Before the flotation, it is necessary to improve the mineral liberation degree of the ore by crushing and/or grinding to improve the flotation efficiency [9,10]. It was reported that the energy consumption during crushing and grinding occupies 50–70% of the whole process, while the energy utilization efficiency is less than 1% and more than 90% of the energy is lost in the form of heat, noise, and so on [11–13]. Therefore, it is critical to develop more efficient and sustainable grinding processes.

Microwave is a type of electromagnetic wave having the frequency within the range 300 MHz–300 GHz. It has the selective and volumetric thermal effects which depend on the microwave absorption capabilities of target materials. It is widely applied for heating to save energy consumption with environmental friendliness, which remains a

big challenge for conventional methods. Currently, microwave radiation had been used in grinding [9,10], drying [14], metallurgy [15], materials synthesis and processing [16,17], and other fields [18,19]. For metal ores, the different microwave absorption capabilities between valuable minerals and gangue minerals lead to dissimilar heating responses, which will create internal stresses and subsequently cracks in the ore in a very short time, i.e., in seconds in many cases [20,21]. These cracks will strengthen the grinding performance of the ore with lower energy consumption by improving mineral liberation. For a copper ore with the grade of 1.7–1.8% after exposure to microwave radiation for 30 s, its grinding time could be reduced by 36.9% and the particle size at 80% of the cumulative distribution (D_{80}) after grinding decreased from 2.00 mm to 1.29 mm [21]. For chalcopyrite ore, its microwave treatment and microflotation test showed that the recovery of chalcopyrite increased from 41% to 51% after microwave treatment for 5 s and decreased to 16% and 4% after the treatment for 10 s and 20 s, respectively, because prolonged microwave treatment time might cause the formation of hydrophilic iron oxides/hydroxides/oxyhydroxides and sulfate species at the chalcopyrite surface, which significantly reduced floatability of the ore [22,23].

Considering the higher processing cost of laterite ore than nickel sulfide ore [24], it is valuable to improve the efficiency of grinding and flotation for strengthening the utilization of nickel sulfide ore. By now, few studies have been conducted on the Jinchuan copper–nickel sulfide ore by focusing on the effect of microwave treatment on the cracking, mineral liberation, and phase composition of the ore [25]. In this study, the microwave absorption capabilities and heating rates of the main minerals in a typical complex copper–nickel sulfide ore in the Jinchuan deposit were investigated. In addition, the effects and mechanisms of microwave treatment on the grinding and flotation characteristics of the ore were evaluated.

2. Experimental

2.1. Raw Materials

The copper–nickel sulfide ore used in this study was taken from the Jinchuan area, Jinchang, China. As shown in Table 1, the contents of Cu and Ni, determined by inductively coupled plasma optical emission spectroscopy (ICP-OES), were 1.24 wt% and 1.27 wt%, respectively. The total contents of other components, mainly MgO, SiO_2, Fe, and S, which were measured by X-ray fluorescence (XRF), exceeded 95 wt%.

Table 1. Main chemical composition of copper–nickel sulfide ore (wt%).

Component	MgO	SiO_2	Al_2O_3	CaO	Fe	S	Cu	Ni
Content	30.26	32.60	2.68	2.50	24.22	9.25	1.24	1.27

Figure 1 shows the XRD pattern of the ore. The main phases of copper–nickel sulfide ore used in this study were lizardite ($Mg_3[(Si,Fe)_2O_5](OH)_4$), cordierite ($Mg_2Al_4Si_5O_{18}$), quartz (SiO_2), amesite ($Mg_2Al[(Si,Al)_2O_5](OH)_4$), chalcopyrite ($CuFeS_2$), pentlandite ($(Fe,Ni)_9S_8$), pyrrhotite ($Fe_7S_8$), and pyrite ($FeS_2$). Its elemental distribution was determined by scanning electron microscopy (SEM)—energy-dispersive spectrometry (EDS) analysis. As shown in Figure 2, Cu, Ni, Fe, and S were the main elements of the target sulfide minerals, i.e., chalcopyrite and pentlandite, while Mg and Si were the primary elements of the gangue minerals. The valuable minerals were tightly bound and wrapped by gangue minerals, indicating the necessity of sufficient ore liberation for subsequent processing. For comparison and microwave heating mechanism analysis, various metal sulfide mineral samples, including chalcopyrite, pyrite, and pyrrhotite, were collected. Figure 3 shows their XRD patterns, which proved their high purity.

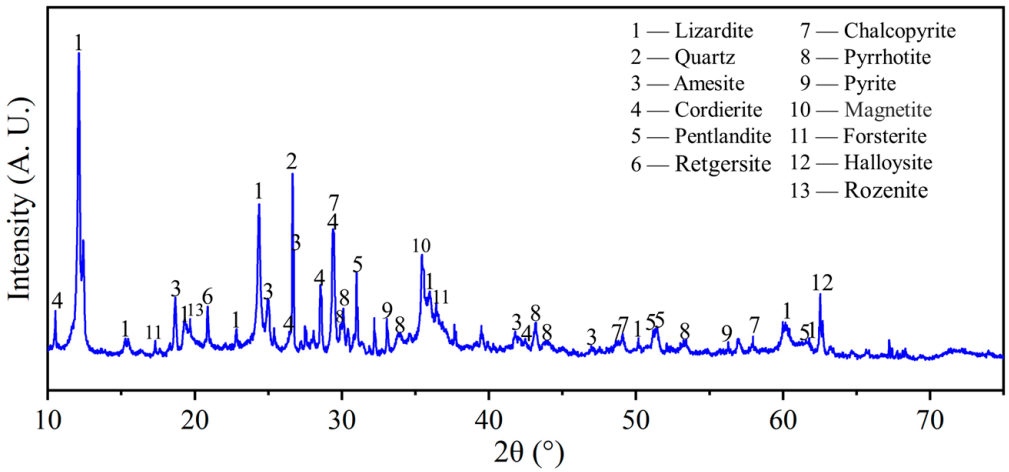

Figure 1. XRD pattern of copper–nickel sulfide ore.

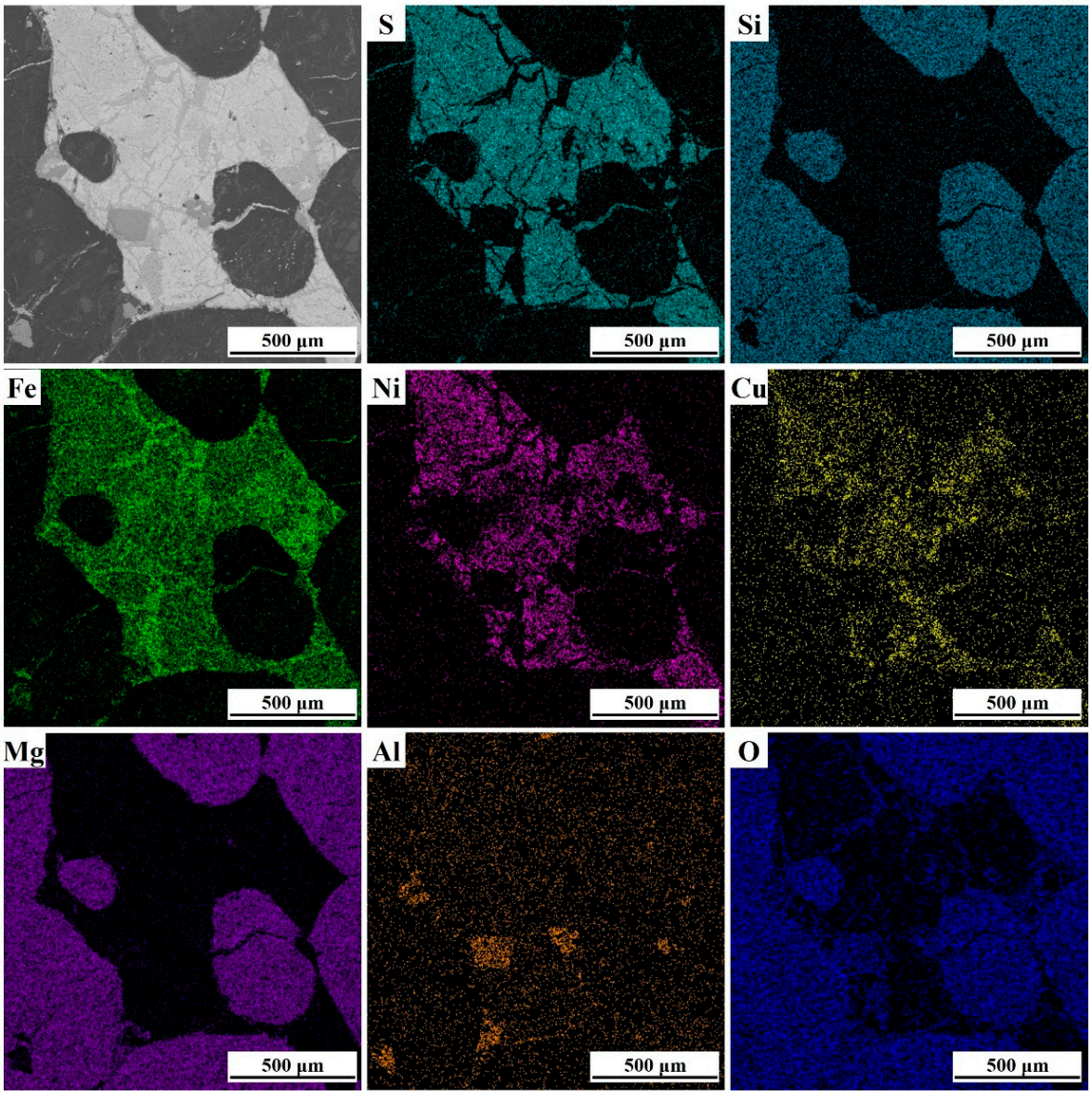

Figure 2. SEM-EDS analysis of copper–nickel sulfide ore.

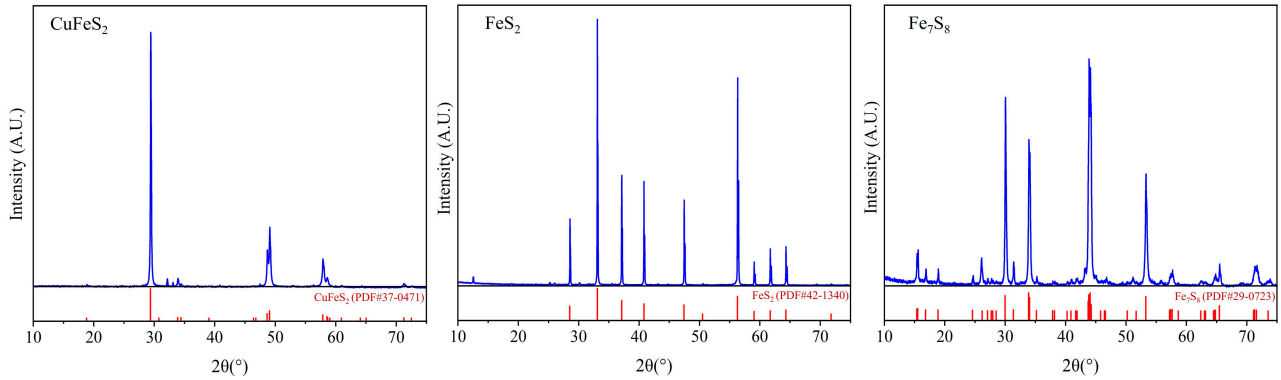

Figure 3. XRD patterns of chalcopyrite, pyrite, and pyrrhotite.

2.2. Experimental Procedure

2.2.1. Thermodynamic Calculation

The variations of standard Gibbs free energy changes of possible reactions ($\Delta_r G_m^\theta$) with temperature (T) during the microwave treatment process of the copper–nickel sulfide ore were calculated using the software FactSage 8.1 (Thermfact/CRCT, Montreal, QC, Canada; GTT-Technologies, Herzogenrath, Germany) to evaluate the feasibility of the reactions.

2.2.2. Microwave Absorption Capability Determination

The permittivities and permeabilities of the ore and the main sulfide minerals, including chalcopyrite, pyrite, and pyrrhotite, were measured firstly by the coaxial method using a vector network analyzer (VNA, E5071C, Agilent Technology Co., Ltd., Santa Clara, CA, USA) in the frequency range 2–4 GHz. Note that pentlandite could be intimated by pyrrhotite with similar properties and the magnetism of chalcopyrite, pyrite, and pyrrhotite would also be beneficial for microwave treatment of the ore, as reported in the literature [20,26–29]. Also, pure gangue minerals related to those in the ore were not prepared for the same measurement because their properties have been reported in detail [8,30–32]. For the measurements, the sample particles with sizes of −0.074 mm were mixed with paraffin wax in a mass ratio of 7/3 and pressed through a pressing machine to make ring samples with an inner diameter of 3 mm, an outer diameter of 7 mm, and a thickness of 2 mm. By using the measured values, the microwave absorption capabilities of the materials could be determined by calculating the corresponding values of microwave penetration depth, D_p, which is defined as the depth at which the microwave power falls to 1/e (e: natural constant) of its original or surface value. Its equation is given as follows [33]:

$$D_p = \frac{\lambda_0}{2\sqrt{2}\pi}\left\{\varepsilon_r''\mu_r'' - \varepsilon_r'\mu_r' + \left[\left(\varepsilon_r'\mu_r'\right)^2 + \left(\varepsilon_r''\mu_r''\right)^2 + \left(\varepsilon_r'\mu_r''\right)^2 + \left(\varepsilon_r''\mu_r'\right)^2\right]^{\frac{1}{2}}\right\}^{-\frac{1}{2}} \quad (1)$$

where λ_0 is the microwave wavelength in free space; ε_r' is the real part of the complex relative permittivity of the material (relative dielectric constant); ε_r'' is the imaginary part of complex relative permittivity of the material (relative dielectric loss factor); μ_r' is the real part of complex relative permeability of the material (relative magnetic constant); and μ_r'' is the imaginary part of the complex relative permeability of the material (relative magnetic loss factor).

2.2.3. Microwave Treatment

Microwave treatment was carried out in a microwave tube furnace (CY-SA1700C-S, Hunan Changyi Microwave Technology Co., Ltd., Changsha, China). By considering the working conditions of the furnace and preliminary experimental results, in each test, 120 g of the ore with a particle size of −1.25 + 0.60 mm was used and placed in a microwave-transparent corundum crucible in the furnace for treatment. The microwave frequency and power were 2.45 GHz and 2200 W, respectively, and the treatment time was set at 0 s,

10 s, 20 s, 30 s, and 40 s, respectively. The temperatures of the samples during microwave treatment were measured by a thermocouple (53IIB, FLUKE Testing Instruments Co., Ltd., Everett, WA, USA), which was inserted inside the samples. After the treatment, the samples were taken out and naturally cooled for characterization and subsequent experiments. The phase compositions of the samples were determined by an X-ray diffraction spectrometer (XRD, D/max 2550PC, Rigaku Co., Ltd., Tokyo, Japan) using a Cu-anode target with the wavelength of 1.54056 Å, step scan mode, and step length of 0.02°. For micro-morphology analysis, the samples were embedded in epoxy glue for fixation and polishing. The microstructures and elemental distributions of the samples were determined by a scanning electron microscope (SEM, MIRA3 LMH, TESCAN, Brno, Czech Republic) equipped with an energy-dispersive X-ray spectrometer (EDS, One Max 20, Oxford Instruments PLC, Oxford, UK). The cracks in the microstructure images were identified and binarized for calculating the percentage of light area as the crack percentage using the Advanced Weka Segmentation module in the software ImageJ 2.0 (National Institutes of Health, Bethesda, MD, USA).

2.2.4. Grinding and Flotation

For grinding, 110 g of microwave-treated ore was ground in a ball mill with a liquid-to-solid ratio of 1 for 14 min. The particle size distributions of the pulps after grinding were determined using a laser particle size analyzer (Malvern Mastersizer 2000, Malvern Panalytical, Malvern, UK). The ground samples were embedded with epoxy resin and polished, as observed and photographed from one field of view after another using an optical microscope (DMI5000M, Leica Instruments Co., Ltd., Mannheim, Germany). Afterwards, according to the area occupied by the target minerals in the ore particles under the microscope which could be classified into five types: 1/5, 2/5, 3/5, 4/5, 1, denoted by $N_{1/5}$, $N_{2/5}$, $N_{3/5}$, $N_{4/5}$, N_1, respectively, the mineral liberation degree (L) was calculated using the following equation.

$$L = \frac{N_1}{N_1 + \frac{1}{5}N_{1/5} + \frac{2}{5}N_{2/5} + \frac{3}{5}N_{3/5} + \frac{4}{5}N_{4/5}} \times 100\% \quad (2)$$

After grinding, the pulp was left to settle for 50 min. After removing the top layer of the clear liquid, the bottom pulp was moved to the flotation cell while the flotation liquid-to-solid ratio was adjusted. Pulp sampling was carried out in the flotation cell using a sampler and multiple pulp sampling was carried out at different locations in the cell to ensure the representativeness of the removed pulp. Before the laser particle size analysis, sodium hexametaphosphate ($(NaPO_3)_6$) was added as a dispersant in the pulp and subjected to ultrasonic treatment for 5 min to avoid the serious agglomeration of the gangue mineral, namely lizardite [5]. To assess the grindability of the ore, the values of relative work index (RWI) were calculated using the following equation [8]:

$$RWI = \left[\left(\frac{10}{\sqrt{P_r}} - \frac{10}{\sqrt{F_r}}\right) \Big/ \left(\frac{10}{\sqrt{P_t}} - \frac{10}{\sqrt{F_t}}\right)\right] \times 100\% \quad (3)$$

where P and F denote the 80% passing sizes of the grinding product and feed ore, respectively; and r and t denote the untreated and treated ores, respectively. A RWI less than 100% indicates an increase in ore grindability and a decrease in ore particle size, while a RWI greater than 100% shows a decrease in ore grindability and an increase in ore size.

The flotation experiments were carried out in a 0.5 L flotation cell with a rotation speed of 2000 rpm and a pulp concentration of 20% during the flotation conditioning stage (XFD IV, Jilin Exploration Machinery Company, Jilin, China). The automatic froth scraping was carried out with an air flow rate of 3.2 L/min and a scraper speed of 30 rpm. Sodium hexametaphosphate ($(NaPO_3)_6$), copper sulfate ($CuSO_4$), butyl sodium xanthate ($C_4H_9OCSSNa$), and terpineol were used as the depressant, activator, collector, and frother, respectively. The pulp pH was 7. Figure 4 shows the flotation flowsheet. It included one

rougher flotation stage for 30 s and four scavenger flotation stages for 30 s, 60 s, 60 s and 60 s, respectively. The corresponding concentrate and middlings were named K, Π_1, Π_2, Π_3, and Π_4, respectively. Correspondingly, the flotation tailing was named X.

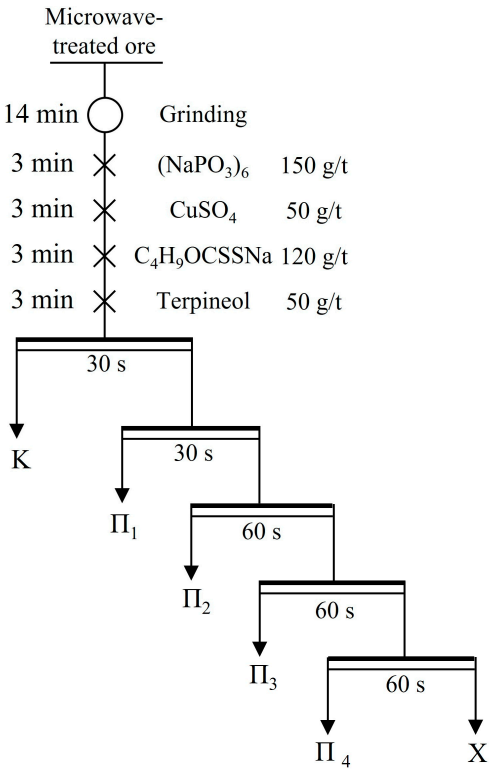

Figure 4. Flotation flowsheet.

The Cu and Ni contents of the samples were measured using an inductively coupled plasma–optical emission spectrometer (ICP-OES, Optima 5300, PerkinElmer, Waltham, MA, USA) before which 0.1000 ± 0.0010 g of each sample was dissolved with aqua regia (volume ratio, HCl/HNO_3 = 3, 30 mL), HF (4 mL), and $HClO_4$ (4 mL) by heating at 140 °C for 30 min and then at 220 °C for 30 min. The metal enrichment ratios, *E*, and recoveries, *R*, of the flotation concentrate, were calculated by Equations (4) and (5), respectively:

$$E = \frac{c}{f} \tag{4}$$

$$R = \frac{\gamma \times c}{f} \times 100\% \tag{5}$$

where *c* is the copper or nickel content in the concentrate; *f* is the copper or nickel content of copper–nickel sulfide ore, and γ is the yield of the concentrate.

The flotation data were fitted using a first-order kinetic model with rectangular distribution of floatability to further investigate the effect of microwave treatment on the flotation behavior [34]. The related equation is given as follows:

$$R = R_\infty \left[1 - \frac{1}{kt}\left(1 - e^{-kt}\right)\right] \tag{6}$$

where *R* is the recovery at the cumulative flotation time *t*; R_∞ is the theoretical maximum recovery; and *k* is the first-order flotation rate constant.

3. Results and Discussion

3.1. Thermodynamic Analysis

To determine the effect of microwave treatment on the phase transformation of the valuable minerals in the ore, the variations of the standard Gibbs free energy changes of the relevant reactions of chalcopyrite, pyrite and pyrrhotite with temperature were determined in the temperature range from 25 °C to 800 °C. Due to the complexity of oxidation behaviors of pentlandite, $(Ni,Fe)_9S_8$, it cannot be calculated directly. Instead, its main preliminary oxidation products, NiS and FeS, were considered [35]. The results are shown in Table 2 and Figure 5. Considering the negative values of $\Delta_rG_m^\theta$ of the reactions at low temperatures, the oxidations of Fe_7S_8, $CuFeS_2$, FeS_2, NiS, and their weak oxidation products (FeS, Cu_2S, etc.) are thermodynamically feasible. The oxidation of $FeSO_4$ and the decomposition of $NiSO_4$ may also occur by elevating temperature.

Table 2. Standard Gibbs free energy changes of the main reactions involved in the treatment of copper–nickel sulfide ore.

No.	Reaction Equation	$\Delta_rG_m^\theta$ − T (kJ/mol)
(7)	$2CuFeS_2(s) + 4O_2(g) = 2FeO(s) + Cu_2S(s) + 3SO_2(g)$	−1117.35 + 0.098T
(8)	$2Cu_2S(s) + 3O_2(g) = 2Cu_2O(s) + 2SO_2(g)$	−708.26 + 0.204T
(9)	$2Cu_2O(s) + O_2(g) = 4CuO(s)$	−220.49 + 0.202T
(10)	$4CuFeS_2(s) + 13O_2(g) = 4CuO(s) + 2Fe_2O_3(s) + 8SO_2(g)$	−3676.19 + 0.859T
(11)	$4Fe_7S_8(s) + 9O_2(g) = 6Fe_2O_3(s) + 16FeS_2(s)$	−4033.94 + 2.619T
(12)	$FeS_2(s) + O_2(g) = FeS(s) + SO_2(g)$	−242.56 −0.064T
(13)	$FeS(s) + 2O_2(g) = FeSO_4(s)$	−729.23 + 0.358T
(14)	$4FeSO_4(s) + O_2(g) = 2Fe_2O_3(s) + 4SO_3(g)$	335.18 − 0.488T
(15)	$4FeS(s) + 7O_2(g) = 4SO_2 + 2Fe_2O_3(s)$	−2286.74 + 0.564T
(16)	$NiS(s) + 2O_2(g) = NiSO_4(s)$	−675.18 + 0.347T
(17)	$2NiS(s) + 3O_2(g) = 2NiO(s) + 2SO_2(g)$	−846.11 + 0.151T
(18)	$NiSO_4(s) = NiO(s) + SO_3(g)$	178.38 − 0.177T

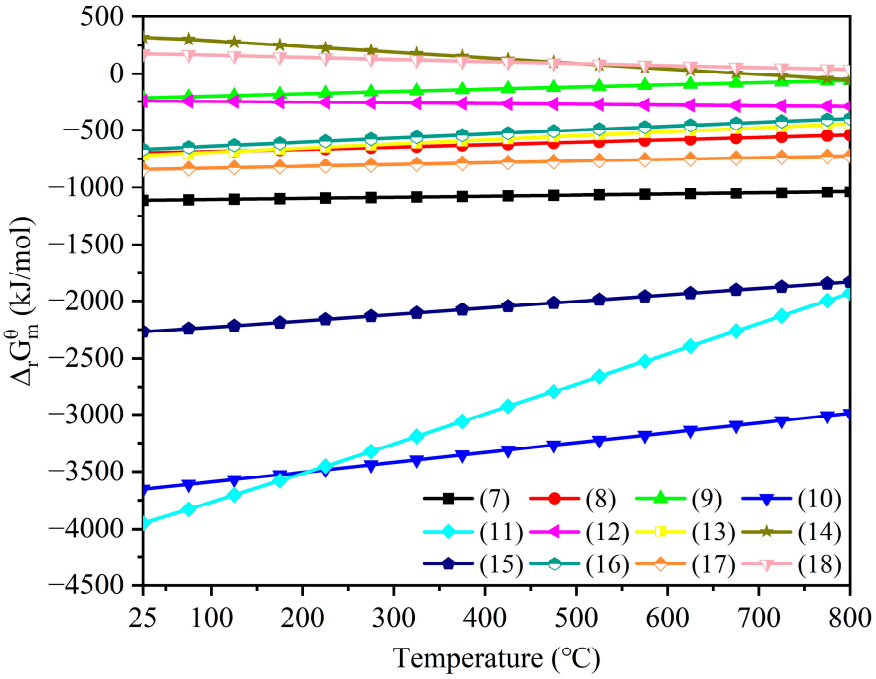

Figure 5. $\Delta_rG_m^\theta$ − T diagram of the main reactions involved in the treatment of copper–nickel sulfide ore.

3.2. Microwave Absorption Capability Analysis

Figure 6 shows the values of the complex relative permittivity and complex relative permeability of copper–nickel sulfide ore, chalcopyrite, pyrite, and pyrrhotite in the fre-

quency range 2.0–4.0 GHz. These parameters remained relatively stable as the frequency varied. Figure 7 shows their D_p values at 2.45 GHz. It was found that the D_p value of copper–nickel sulfide ore was 20.57 mm, higher than those of chalcopyrite, pyrite, and pyrrhotite (all around 15 mm). It indicated the better microwave absorption capabilities of the metal sulfide minerals than that of the ore itself. This was because the ore contained both metal sulfide minerals and gangue minerals, such as magnesium or aluminum silicates, which were considered to be nearly microwave-transparent at room temperature, as verified by the measurements of their electromagnetic properties and heating rates [30–32]. Obviously, due to the significant differences of microwave absorption capabilities between the minerals, they would have different microwave heating characteristics.

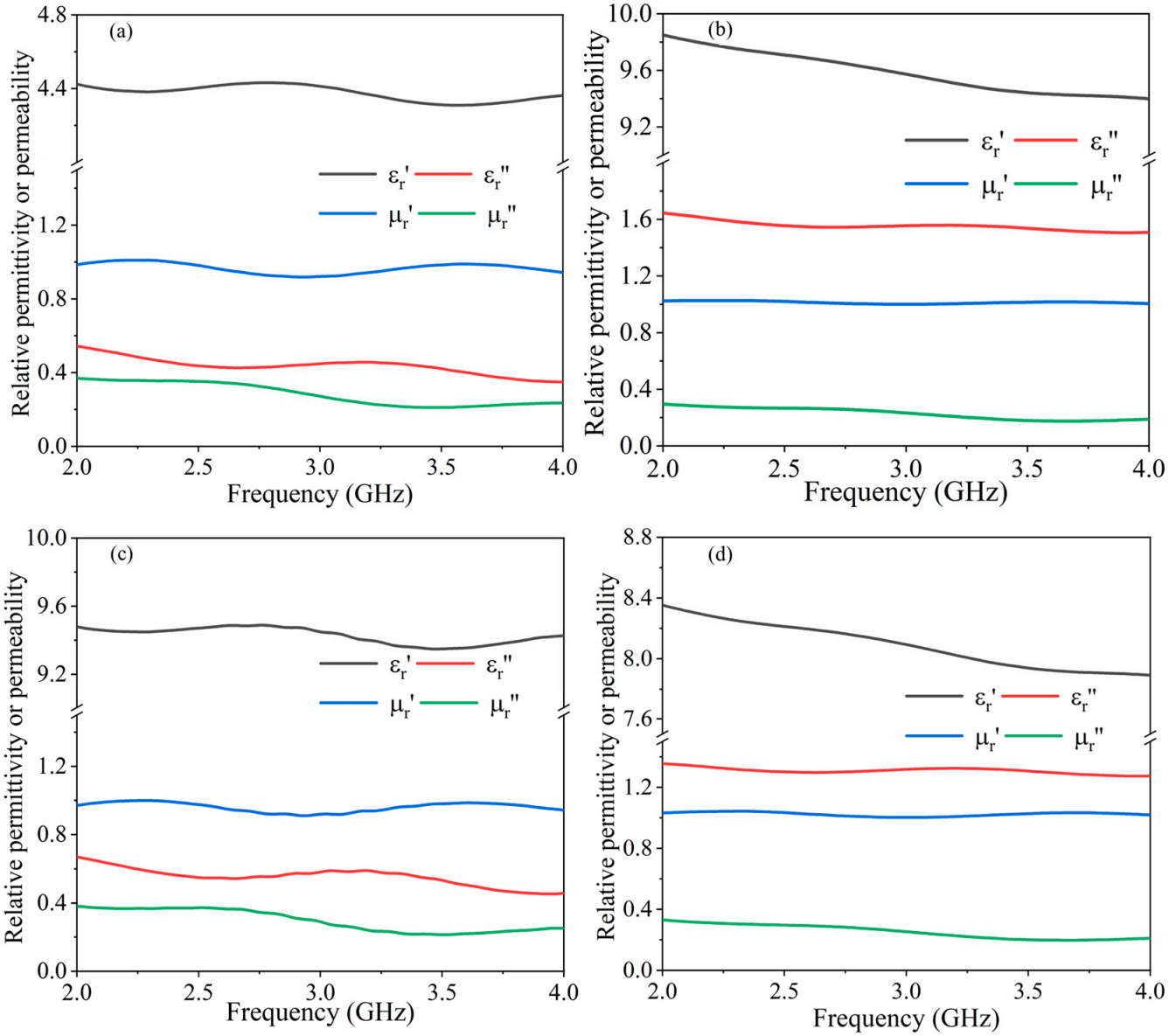

Figure 6. Complex relative permittivities and permeabilities of (**a**) copper–nickel sulfide ore, (**b**) chalcopyrite, (**c**) pyrite, and (**d**) pyrrhotite.

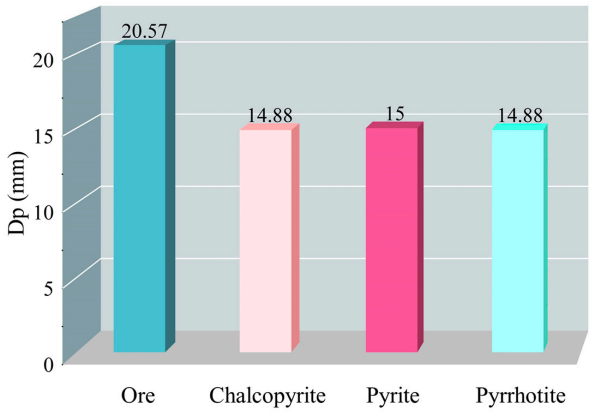

Figure 7. D_p values of copper–nickel sulfide ore and different minerals at 2.45 GHz.

3.3. Microwave Treatment Analysis

3.3.1. Microwave Heating Characteristics

Figure 8 shows the temperature changes of copper–nickel sulfide ore and different minerals as a function of microwave treatment time. As shown in Figure 8, in the early stage of microwave treatment (0–15 s), the differences in temperature between the ore and minerals kept increasing. Pyrite, chalcopyrite, and pyrrhotite had higher heating rates than the ore due to their better microwave absorption capabilities than the ore at low temperature, as proven in Figure 7. After microwave treatment for 15–20 s, their temperature increasing trends became slower due to possible oxidation reactions. It indicated that further extending the treatment time may not be conducive to improving the overall efficiency of grinding and flotation. Unlike the above minerals, the gangue mineral, lizardite, had a lower microwave heating rate. The maximum temperature difference between sulfide minerals and gangue minerals could reach 418 °C (chalcopyrite vs. lizardite) after microwave treatment for 20 s. The significant temperature differences between the minerals under microwave irradiation provided the feasibility of microwave-assisted grinding. For other gangue minerals, including cordierite and amesite, they showed poor heating performance with minor temperature changes, even after 60 s. Obviously, they were nearly microwave-transparent.

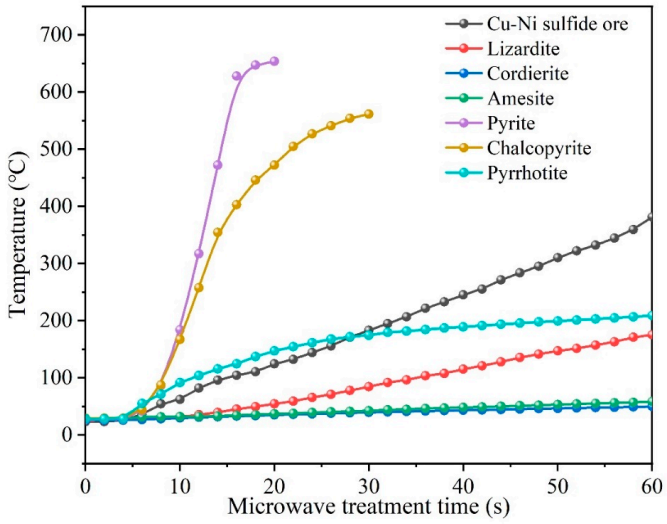

Figure 8. Temperature rising curves of the ore and different minerals during microwave treatment.

Along with the temperature increase during microwave treatment, the structure of the ore would also change. As shown in Figure 9a, obvious macroscopic cracks were produced on the ore surfaces after microwave treatment. Figure 9b shows the microstructure and spot compositions of the ore sample obtained after microwave treatment for 20 s. The obvious

cracks appeared on the boundaries of the bright and dark areas and inside them. The main elements in the dark gray area of Figure 9b (spot C) were Mg and Si, indicating the existence of silicates. The light gray area (spot B) was mainly composed of Fe, S, and O, indicating the presence of pyrite and iron oxide. The bright area (spot A) was constituted by Cu, Fe, and S, which were probably the components of chalcopyrite. Figure 10 shows some representative SEM images of internal cracks in the ore after microwave treatment. As the microwave treatment time was extended, the quantity and size of cracks in the ore increased.

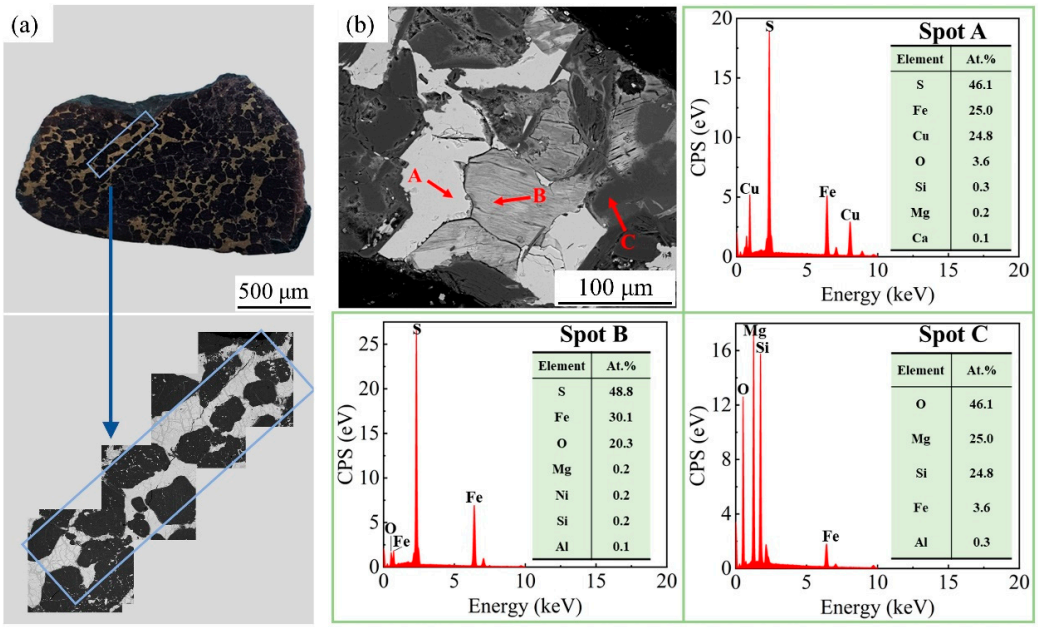

Figure 9. (**a**) Macroscopic cracks in the copper–nickel sulfide ore and (**b**) the microstructure of copper–nickel sulfide ore with EDS analysis.

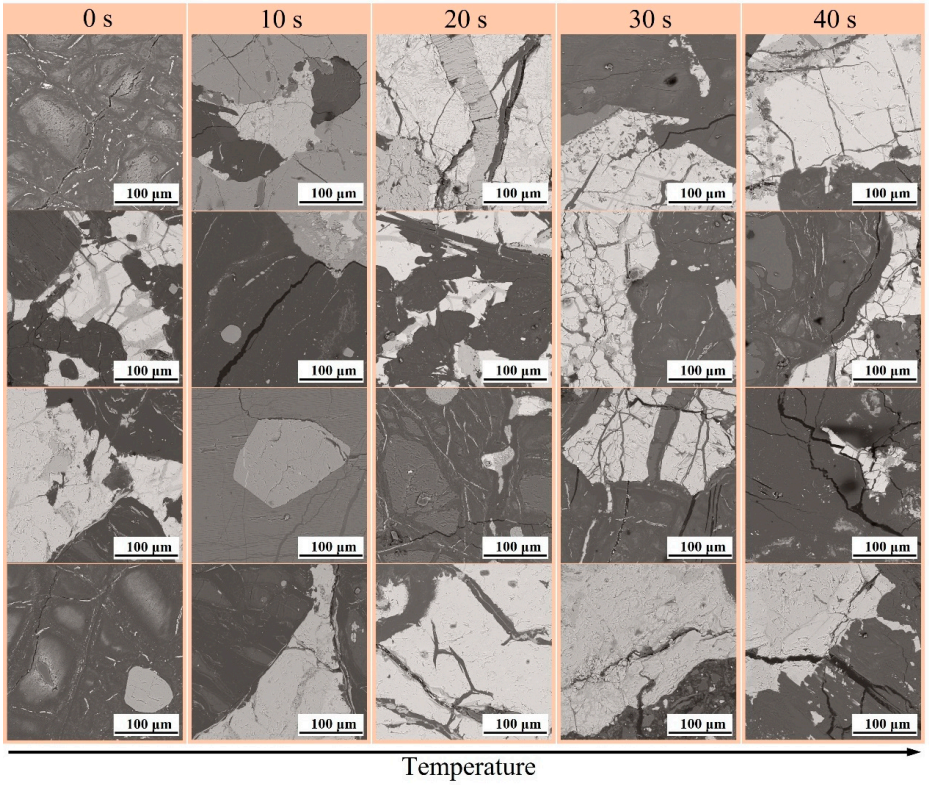

Figure 10. Representative SEM images of the ore after microwave treatment for different time.

3.3.2. Grinding Characteristics of Ore

The crack percentages of the ore samples treated for different time were statistically analyzed. As shown in Figure 11, the crack percentage increased with microwave treatment time. The results indicated that microwave treatment promoted the formation of cracks between different minerals in the ore, as observed from the binarized images of ore cracks after microwave treatment in Figure 12. The cracks would effectively intensify mineral liberation. Figure 13 shows the variation of liberation degree of Cu/Ni-bearing minerals, including chalcopyrite and pentlandite, in the ore with microwave treatment time. It was obvious that the liberation degree increased with the extension of microwave treatment time. However, after microwave treatment for over 20 s, their liberation degrees increased minorly because the quantity of the cracks gradually reached the maximum.

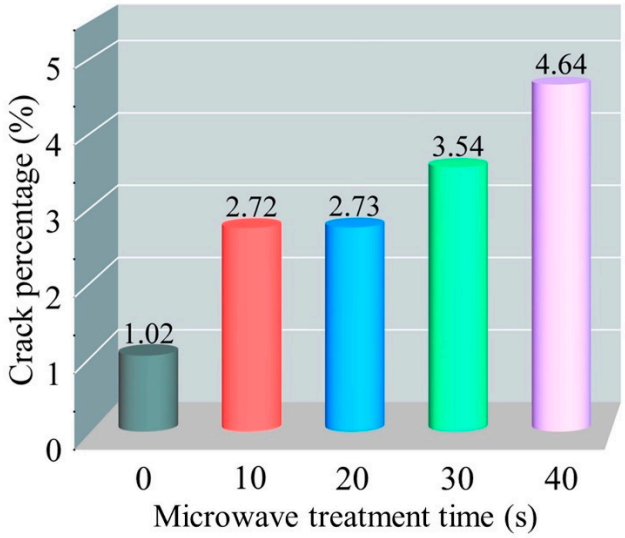

Figure 11. Effect of microwave treatment time on the crack percentage of the ore.

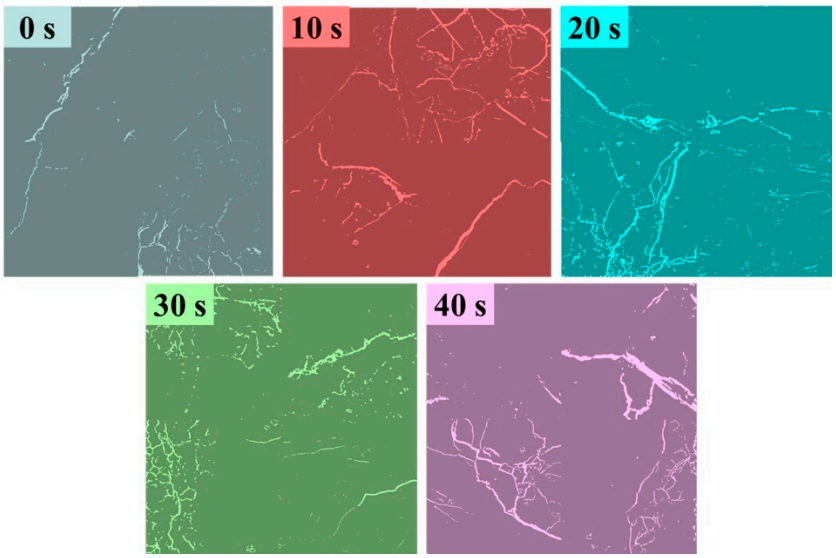

Figure 12. Representative binarized images of ore cracks after microwave treatment.

Figure 14 shows the variation of the particle size distribution of the microwave-treated ore after grinding with microwave treatment time. The particle size differential distribution curves showed two peaks in the size ranges 20–100 μm and 0.1–1 μm. Meanwhile, the cumulative size distribution curve moved to the left with increasing microwave treatment time. Correspondingly, the particle size corresponding to the highest peak of the particle

size differential distribution curve decreased while the percentage of −0.074 mm particles increased. These changes indicated that microwave treatment reduced the overall particle size and promoted the particle size uniformity, which was beneficial for mineral liberation. From the curves, the values of D_{10}, D_{50}, and D_{90} (particle sizes at 10%, 50% and 90% of the cumulative distribution, respectively) could be determined, as summarized in Table 3. It was obvious that they kept decreasing with increasing microwave treatment time.

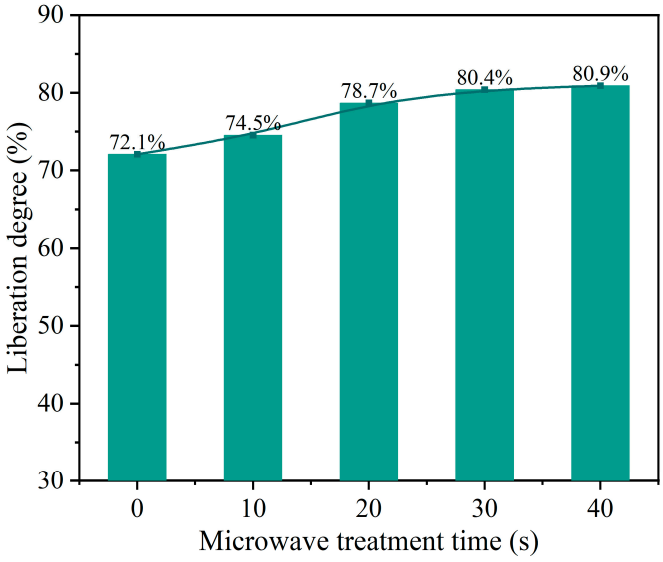

Figure 13. Effect of microwave treatment time on the liberation degree of Cu/Ni-bearing minerals.

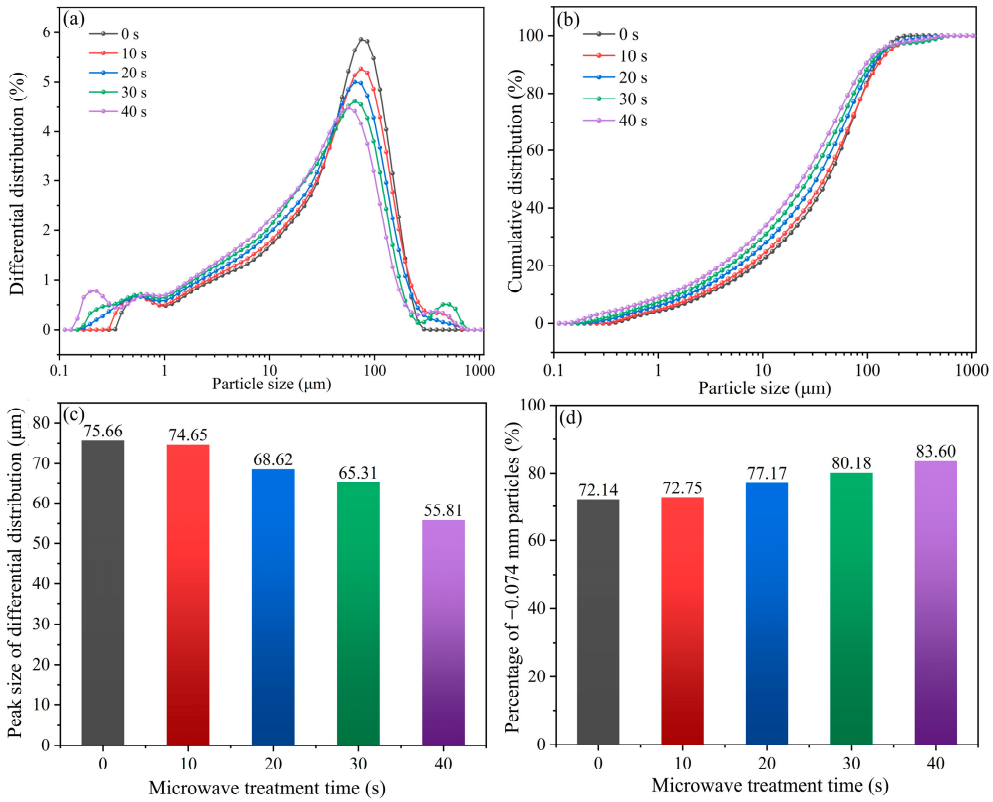

Figure 14. Particle size distribution analysis of the microwave-treated ore after grinding: (**a**) differential distribution, (**b**) cumulative distribution, (**c**) peak sizes determined from differential distribution, and (**d**) percentages of −0.074 mm particles determined from cumulative distribution.

Table 3. Particle size percentages of microwave-treated ore after grinding.

Treatment Time (s)	Particle Size Percentage (%)		
	D_{10}	D_{50}	D_{90}
0	3.011	44.687	126.984
10	2.644	41.252	134.195
20	2.061	34.985	120.777
30	1.673	29.292	112.642
40	1.286	25.469	101.980

It should be noted that the production amount of fine particles in the pulp during grinding should be appropriate. With excessive fine particles, a serious sliming phenomenon would occur, causing the excessive adhesion of gangue minerals to the surface of target minerals. As a result, it would lower the metal recovery. For instance, the heteroaggregation between lizardite and pentlandite would take place [36], reducing the Ni recovery in the concentrate.

The D_{80} and RWI of the ores after microwave treatment for 10 s were almost unchanged compared to the untreated ore (Figure 15). When the treatment time reached 20 s, there were significant decreases in D_{80} and RWI, showing better grindability. In particular, the corresponding RWI decreased by 11.5%. When the treatment time reached 40 s, the RWI decreased to nearly 70% of the untreated sample, which indicated a significant decrease in the grinding energy consumption.

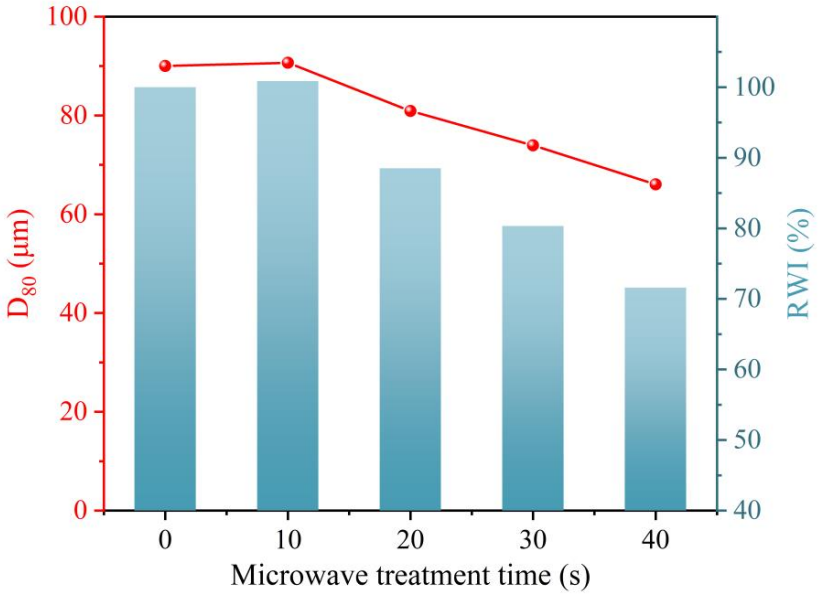

Figure 15. Effect of microwave treatment time on D_{80} and RWI.

3.3.3. Flotation Characteristics of Ground Ore

Figure 16 shows the effect of microwave treatment time on the enrichment ratios and recoveries of Cu and Ni in the flotation concentrate. After microwave treatment for 10 s, both the enrichment ratios and recoveries of Cu and Ni in the concentrate decreased compared to the untreated sample. However, by extending the time to 20 s, the flotation performance improved significantly. The enrichment ratios of Cu and Ni increased by 0.3 and 0.2, respectively, and the recoveries of Cu and Ni increased by 4.2% and 3.1%, respectively, as compared to those of the untreated sample. With a further increase in microwave treatment time, the changes in enrichment ratios and recoveries of Cu and Ni became less considerable. When the treatment time reached 40 s, the recoveries of Cu and Ni decreased by 6.67% and 11.11%, respectively, compared to those of the untreated ore.

Note that the variations of the indexes for Ni were greater than those for Cu due to the stronger heteroaggregation between lizardite and pentlandite [36].

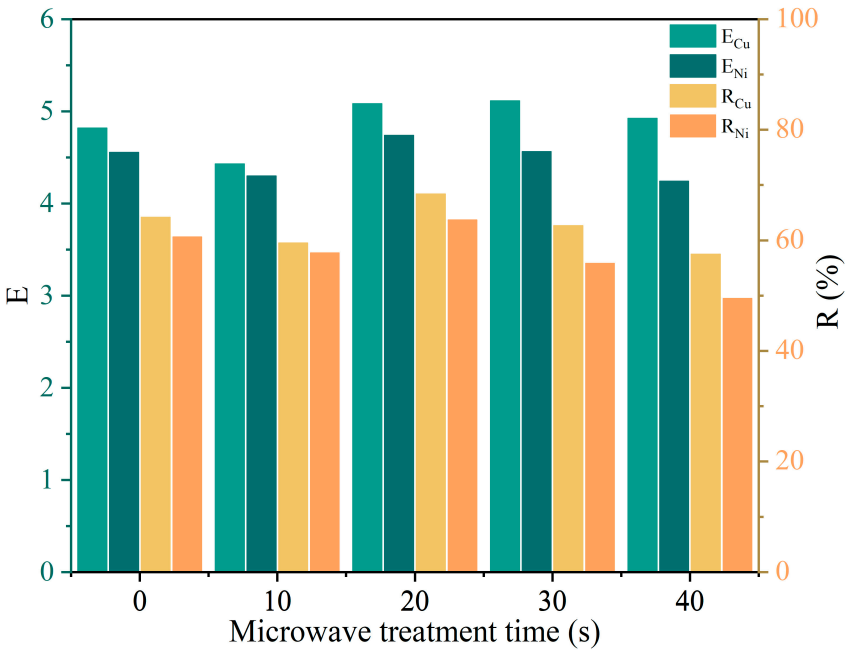

Figure 16. Effect of microwave treatment time on the enrichment ratios and recoveries of Cu and Ni in the flotation concentrate.

Figure 17 shows the flotation data fitting curves from which the corresponding values of k, R_∞, and R^2 (coefficient of determination) were determined. According to Table 4, all R^2 were greater than 0.999 and the results were considered reliable. The changes in R_∞ of Cu and Ni had similar trends after microwave treatment. The value of R_∞ of the ore after microwave treatment for 20 s was higher than that of the untreated ore. When the treatment time exceeded 20 s, the values of both R_∞ and k decreased. It indicated that the oxidation caused by the prolonged microwave treatment degraded the flotation performance. It should be mentioned that the value of k of the microwave-treated ore was smaller than that of the untreated ore in the initial stage of flotation, due to the increase in the content of micro-fine particles in the pulp, in which more gangue mineral particles adhered to the concentrate surface.

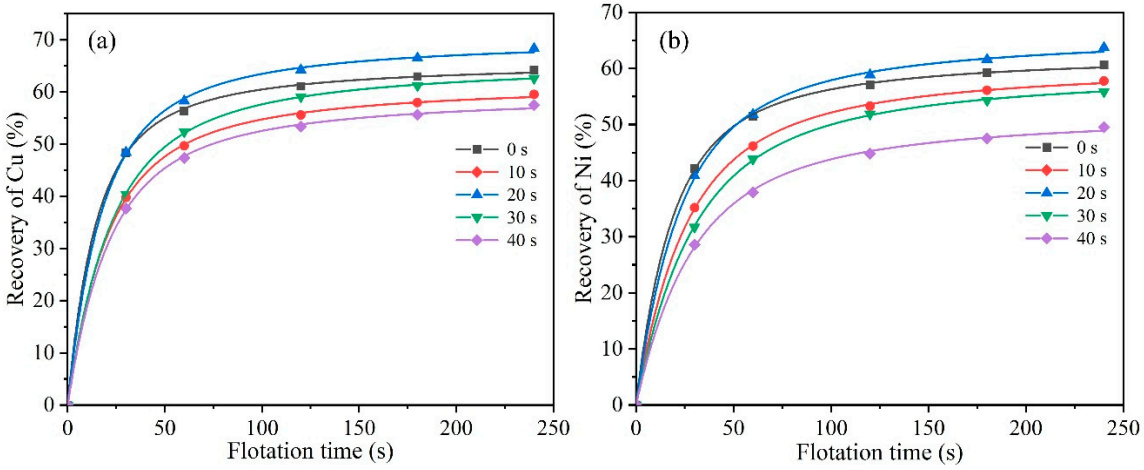

Figure 17. Fitting of flotation data using the first-order kinetic model with rectangular distribution of floatability: (**a**) recovery of Cu and (**b**) recovery of Ni.

Table 4. Fitting parameters of the first-order kinetic model with rectangular distribution of floatability.

Treatment Time (s)	k (s^{-1})		R_∞ (%)		R^2	
	Cu	Ni	Cu	Ni	Cu	Ni
0	0.11967	0.09368	65.982	62.994	0.99982	0.99983
10	0.08444	0.06761	62.083	61.163	0.99981	0.99987
20	0.09912	0.07631	70.576	66.618	0.99966	0.99960
30	0.07777	0.05887	66.116	60.173	0.99994	0.99992
40	0.08081	0.05986	59.945	52.561	0.99969	0.99946

The variations of the above flotation indexes were attributed to the phase transformation during microwave treatment. Figure 18 shows the XRD patterns of the copper–nickel sulfide ore after microwave treatment for different time. After microwave treatment for 10 s, mackinawite (FeS) and cuprite (Cu_2O) were formed, with the increase in retgersite ($NiSO_4 \cdot 6H_2O$) and decrease in pentlandite due to its oxidation. After treatment time was extended to 20 s, more mackinawite was found, with less cuprite and retgersite because of further oxidation. As the treatment time increased to 40 s, all these phases decreased gradually. Moreover, rozenite ($FeSO_4 \cdot 4H_2O$) kept decreasing throughout microwave treatment, presumably following an oxidative reaction to Fe (III) sulfates [37]. Clearly, by microwave treatment, the ore began to oxidize within a short time. With the prolongation of treatment time, the oxidation would continue with the rate affected by the consumption of internal oxygen.

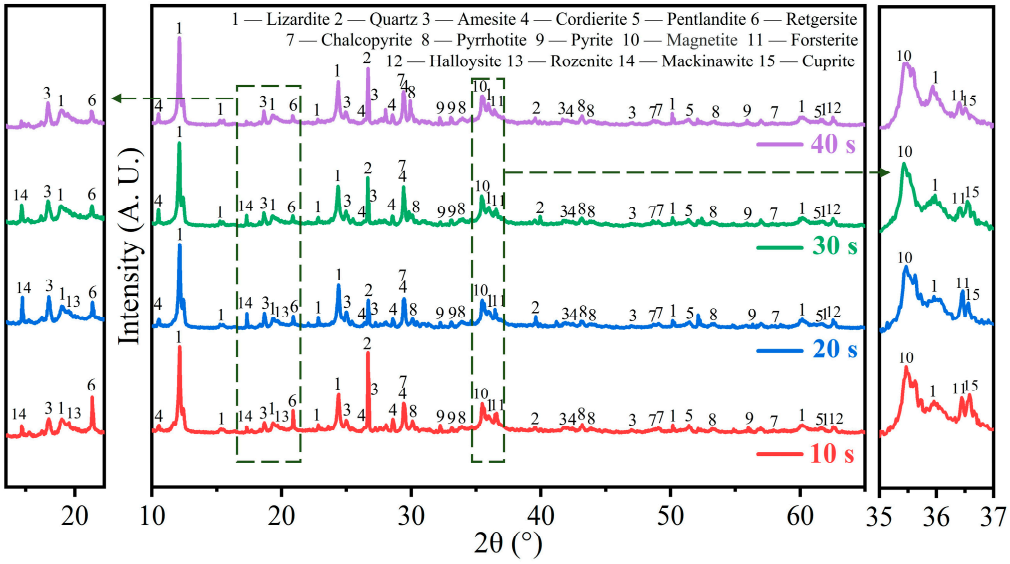

Figure 18. XRD patterns of copper–nickel sulfide ore after microwave treatment for different time.

Based on the above findings, the influence of microwave treatment on the flotation performance depended on the competition between the positive effect of the liberation of sulfide minerals and the negative effect of the oxidation of the minerals. Initially, the mineral liberation and oxidation in the ore were limited, leading to the relatively low metal recoveries after flotation. As the treatment time was extended to 20 s, the enhanced liberation and moderate oxidation of sulfide minerals under microwave irradiation contributed to the better flotation indexes. As the microwave treatment time increased continuously, the oxidation of sulfide minerals became excessive and deteriorated the flotation performance.

4. Conclusions

This study focused on the influence of microwave treatment on the grinding and flotation performance of the copper–nickel sulfide ore based on the determination of its

microwave absorption capability, grinding and flotation indexes such as crack percentage, mineral liberation degree, particle size distribution, RWI, metal enrichment ratio and recovery. By measuring the electromagnetic properties, the microwave penetration depths of the ore and its main minerals were determined to confirm their different microwave absorption capabilities, which led to dissimilar microwave heating characteristics. The maximum temperature difference between the sulfide minerals and gangue minerals could reach 418 °C (chalcopyrite vs. lizardite) after microwave treatment for 20 s. The significant temperature differences between the minerals in microwave treatment provided the feasibility of microwave-assisted grinding. It was demonstrated that microwave treatment could effectively improve the ore grindability, as indicated by the increase in fine particles smaller than 0.074 mm and the decrease in RWI after grinding due to higher crack percentage and mineral liberation degree. It also affected the ore floatability because of the generation of cuprite, retgersite, and rozenite with poor floatability when the treatment time was extended. By microwave treatment for proper time, namely 20 s, the RWI of the ore decreased by 11.5%. After flotation, the enrichment ratios of Cu and Ni in the flotation concentrate increased by 0.3 and 0.2, respectively, and the recoveries of Cu and Ni increased by 4.2% and 3.1%, respectively. The findings can serve as a valuable reference for large-scale microwave processing of sulfide ores.

Author Contributions: Conceptualization, formal analysis, investigation, writing—original draft, visualization, X.F.; resources, supervision, writing—review and editing, Z.P.; formal analysis, investigation, T.Y.; visualization, methodology, M.R.; formal analysis, resources, G.L. All authors have read and agreed to the published version of the manuscript.

Funding: This work was partially supported by the Postgraduate Scientific Research Innovation Project of Hunan Province under Grant CX20220217.

Institutional Review Board Statement: Not applicable.

Informed Consent Statement: Not applicable.

Data Availability Statement: The raw data supporting the conclusions of this article will be made available by the authors on request.

Conflicts of Interest: The authors declare no conflict of interest.

References

1. Hui, S.; Li, B.; Zhou, S.; Wei, Y. Extraction of ferronickel concentrate from laterite nickel ore by reduction roasting-magnetic separation using spent cathode carbon. *Miner. Eng.* **2023**, *201*, 108194. [CrossRef]
2. Zaiman, N.F.H.N.; Shaari, N. Review on flower-like structure nickel based catalyst in fuel cell application. *J. Ind. Eng. Chem.* **2023**, *119*, 1–76. [CrossRef]
3. Golroudbary, S.R.; Kraslawski, A.; Wilson, B.P.; Lundström, M. Assessment of environmental sustainability of nickel required for mobility transition. *Front. Chem. Eng.* **2023**, *4*, 978842. [CrossRef]
4. Mudd, G.M.; Jowitti, S.M. A detailed assessment of global nickel resource trends and endowments. *Econ. Geol.* **2014**, *109*, 1813–1841. [CrossRef]
5. Liu, M.; Su, S.; Yao, Y.; Wu, X.; Cai, N.; Guan, Q. Discovery and genesis of two types of olivines and its significance to metallogeny in Jinchuan magmatic copper-nickel (PGE) sulfide deposit. *Acta Petrol. Sin.* **2020**, *36*, 1151–1170.
6. Faris, N.; Pownceby, M.I.; Bruckard, W.J.; Chen, M. The direct leaching of nickel sulfide flotation concentrates—A historic and state-of-the-art review part I: Piloted processes and commercial operations. *Miner. Process. Extr. Metall. Rev.* **2022**, *44*, 407–435. [CrossRef]
7. Forster, J.; Elliott, R.; Boucher, D.; Bobicki, E.R. High-temperature microwave properties and phase transitions of ultramafic nickel ores. *Miner. Eng.* **2021**, *172*, 107109. [CrossRef]
8. Bobicki, E.R.; Liu, Q.; Xu, Z. Microwave treatment of ultramafic nickel ores: Heating behavior, mineralogy, and comminution effects. *Minerals* **2018**, *8*, 524. [CrossRef]
9. Cai, X.; Qian, G.; Zhang, B.; Chen, Q.; Hu, C. Selective liberation of high-phosphorous oolitic hematite assisted by microwave processing and acid leaching. *Minerals* **2018**, *8*, 245. [CrossRef]
10. Yu, Q.; Ding, D.; Chen, W.; Hu, N.; Wu, L.; Zhang, Q.; Liu, Y.; Zhang, Z.; Li, F.; Xue, X.; et al. Effect of microwave pretreatment on grindability of lead-zinc ore. *Geofluids* **2021**, *2021*, 4418684. [CrossRef]
11. Toifl, M.; Hartlieb, P.; Meisels, R.; Antretter, T.; Kuchar, F. Numerical study of the influence of irradiation parameters on the microwave-induced stresses in granite. *Miner. Eng.* **2017**, *103*, 78–92. [CrossRef]

12. Adewuyi, S.O.; Ahmed, H.A.M.; Ahmed, H.M.A. Methods of ore pretreatment for comminution energy reduction. *Minerals* **2020**, *10*, 423. [CrossRef]
13. Somani, A.; Nandi, T.K.; Pal, S.K.; Majumder, A.K. Pre-treatment of rocks prior to comminution—A critical review of present practices. *Int. J. Min. Sci. Technol.* **2017**, *27*, 339–348. [CrossRef]
14. Zhang, J.; Peng, Z.; Luo, G.; Tian, R.; Rao, M. Microwave drying kinetics of chromium-rich electroplating sludge. *Metals* **2023**, *13*, 87. [CrossRef]
15. Ye, L.; Peng, Z.; Tian, R.; Tang, H.; Zhang, J.; Rao, M.; Li, G. A novel process for highly efficient separation of boron and iron from ludwigite ore based on low-temperature microwave roasting. *Powder Technol.* **2022**, *410*, 117848. [CrossRef]
16. Zhu, G.; Peng, Z.; Yang, L.; Tang, H.; Fang, X.; Rao, M. Facile preparation of thermal insulation materials by microwave sintering of ferronickel slag and fly ash cenosphere. *Ceram. Int.* **2023**, *49*, 11978–11988. [CrossRef]
17. Tang, H.; Peng, Z.; Shang, W.; Ye, L.; Luo, J.; Rao, M.; Li, G. Preparation of refractory materials from electric furnace ferronickel slag and blast furnace ferronickel slag: A comparison. *J. Environ. Chem. Eng.* **2022**, *10*, 107929. [CrossRef]
18. Lin, F.; Feng, X.; Yang, C.; Li, S.; Zhang, J.; Su, X.; Tong, T. Experimental study on improving mechanical mining efficiency of deep banded iron ore by microwave presplitting. *Int. J. Rock Mech. Min. Sci.* **2022**, *159*, 105233. [CrossRef]
19. Hartlieb, P.; Kuchar, F.; Moser, P.; Kargl, H.; Restner, U. Reaction of different rock types to low-power (3.2 kW) microwave irradiation in a multimode cavity. *Miner. Eng.* **2018**, *118*, 37–51. [CrossRef]
20. Goldbaum, M.W.; Elliott, R.; Forster, J.; Maham, Y.; Bobicki, E.R. Investigating the microwave heating behaviour of pyrrhotite tailings. *Miner. Eng.* **2020**, *146*, 106152. [CrossRef]
21. Lin, F.; Feng, X.; Lu, G.; Su, X.; Li, S.; Zhang, J. Study on microwave heating order and electromagnetic characteristics of copper and gold ores. *Rock. Mech. Rock. Eng.* **2021**, *54*, 2129–2143. [CrossRef]
22. da Silva, G.R.; Espiritu, E.R.L.; Mohammadi-Jam, S.; Waters, K.E. Surface characterization of microwave-treated chalcopyrite. *Colloids Surf. A Physicochem. Eng. Asp.* **2018**, *555*, 407–417. [CrossRef]
23. Gholami, H.; Rezai, B.; Hassanzadeh, A.; Mehdilo, A.; Yarahmadi, M. Effect of microwave pretreatment on grinding and flotation kinetics of copper complex ore. *Int. J. Miner. Metall. Mater.* **2021**, *28*, 1887–1897. [CrossRef]
24. Seiler, S.; Sánchez, G.; Pawlik, M.; Bradshaw, P.; Klein, B. Awaruite, a new large nickel resource: Flotation under weakly acidic conditions. *Minerals* **2023**, *13*, 1147. [CrossRef]
25. Li, X.; Tian, S.; Niu, Y.; Lu, B.; Ma, Y.; Xie, X.; Huang, L.; Sun, X.; Ju, S. An experimental study on microwave-assisted grinding and flotation of nickel-copper ore. *J. Kunming Univ. Sci. Technol. (Nat. Sci.)* **2022**, *47*, 7–17.
26. Liu, D.; Zhang, G.; Liu, J.; Pan, G.; Chen, Y.; Wang, M. Studies on the surface oxidation and its role in the flotation of mixed copper-nickel sulfide ore. *Powder Technol.* **2021**, *381*, 576–584. [CrossRef]
27. Kim, B.; Park, J.; Lee, J. Dielectric properites of iron sulfide in coal by microwave irradiation. *J. Korean Soc. Miner. Energy Resour. Eng.* **2013**, *50*, 838–847. [CrossRef]
28. Prameena, B.; Anbalagan, G.; Gunasekaran, S.; Ramkumaar, G.R.; Gowtham, B. Structural, optical, electron paramagnetic, thermal and dielectric characterization of chalcopyrite. *Spectrochim. Acta Part A Mol. Biomol. Spectrosc.* **2014**, *122*, 348–355. [CrossRef] [PubMed]
29. Pearce, C.I. Electrical and magnetic properties of sulfides. *Rev. Mineral. Geochem.* **2006**, *61*, 127–180. [CrossRef]
30. Forster, J.; Maham, Y.; Bobicki, E.R. Microwave heating of magnesium silicate minerals. *Powder Technol.* **2018**, *339*, 1–7. [CrossRef]
31. Ohsato, H.; Terada, M.; Kagomiya, I.; Kawamura, K.; Kakimoto, K.; Kim, E.S. Sintering conditions of cordierite for microwave/millimeterwave dielectrics. *IEEE Trans. Ultrason. Ferroelectr. Freq. Control* **2008**, *55*, 1081–1085. [CrossRef] [PubMed]
32. Lou, W.; Mao, M.; Song, K.; Xu, K.; Liu, B.; Li, W.; Yang, B.; Qi, Z.; Zhao, J.; Sun, S.; et al. Low permittivity cordierite-based microwave dielectric ceramics for 5G/6G telecommunications. *J. Eur. Ceram. Soc.* **2022**, *42*, 2820–2826. [CrossRef]
33. Peng, Z.; Hwang, J.Y.; Mouris, J.; Hutcheon, R.; Huang, X. Microwave penetration depth in materials with non-zero magnetic susceptibility. *ISIJ Int.* **2010**, *50*, 1590–1596. [CrossRef]
34. Vinnett, L.; Waters, K.E. Representation of kinetics models in batch flotation as distributed first-order reactions. *Minerals* **2020**, *10*, 913. [CrossRef]
35. Yu, D.; Utigard, T.A. TG/DTA study on the oxidation of nickel concentrate. *Thermochim. Acta* **2012**, *533*, 56–65. [CrossRef]
36. Feng, B.; Feng, Q.; Lu, Y. A novel method to limit the detrimental effect of serpentine on the flotation of pentlandite. *Int. J. Miner. Process* **2012**, *114*, 11–13. [CrossRef]
37. Xu, L.; Xie, Q.; Chen, T.; Li, P.; Yang, Y.; Zhou, Y. Constraint of nanometer-sized pyrite crystals on oxidation kinetics and weathering products. *J. Nanosci. Nanotechnol.* **2017**, *17*, 6962–6966. [CrossRef]